

Singular Band Behavior of the Extended Emery Model for High- T_c Superconductors

Ivana Mrkonjić and Slaven Barišić

Department of Physics, University of Zagreb, Bijenička 32, POB 331, 10002 Zagreb, Croatia
(February 20, 2001.)

The three band structure of the extended Emery model for the copper-oxide layered materials is analyzed for all the values of the effective tight-binding parameters. The model is characterized by the Cu-O site energy splitting, the Cu-O first neighbor hopping and the O-O second neighbor hopping. For the sufficiently large O-O hoppings, the two bands can come together at one point on the diagonal of the square Brillouin zone, but they cannot cross. The range of the parameters for which the band touching occurs is determined. The model relates the band touching at the bottom of the two bands to the appearance of the extended, one-dimensional-like van Hove singularity at the lower edge of the density of states. With $1 + \delta$ holes (δ small) the extended van Hove singularity can thus occur close to the Fermi level only if the latter cuts two bands. The topology of the Fermi surfaces observed by ARPES in the high- T_c superconductors eliminates such possibility. The Fermi surfaces in LSCO, Bi2212 and Y123 are then fitted with the one of the three bands at the Fermi level. The agreement is excellent considering in particular the fact that the fits use only two parameters. The departure of the measured band structure from the three band prediction found on the small energy scales away from the Fermi level is attributed to the effects of the fluctuations not included into the energy scales which define the three band structure.

I. INTRODUCTION

ARPES measurements of $\text{YBa}_2\text{Cu}_3\text{O}_{6.95}$ (Y123) [1,2], $\text{YBa}_2\text{Cu}_4\text{O}_8$ (Y124) [3], $\text{Bi}_2\text{Sr}_2\text{CaCu}_2\text{O}_{8+\delta}$ (Bi2212) [4–9] and $\text{La}_{2-x}\text{Sr}_x\text{CuO}_4$ (LSCO) [10,11] Fermi surfaces provide interesting information about the qualitative properties of the electron system in the high T_c materials. At least roughly, the electrons behave as fermions with large Fermi surfaces which pass through the vicinity of the hyperbolic van Hove points of the Brillouin zone (BZ), in agreement with some early theoretical conjectures [12,13]. Additionally, the Fermi surface is unusually flat along one of the high symmetry directions passing through the hyperbolic van Hove point. This corresponds to the increase of the strength of the logarithmic van Hove singularity in the electron density of states. Related to it is the early theoretical proposal of the extended (one-dimensional) van Hove singularities [3,14,15], which are stronger than logarithmic.

The experimentally obtained \mathbf{k} -dependence of the conducting band is usually fitted throughout the BZ with the Fourier series involving only the first and second harmonics in the symmetry allowed combinations [1,16]. Such fits use six independent parameters and they suggest in particular that the direct oxygen-oxygen hopping is small, but not negligible with respect to the direct copper-oxygen hopping of the electrons. The former procedure is unjustly called "tight-binding" fits.

Actually, the proper tight-binding calculation with one copper state and two oxygen states per unit cell leads to the three band structure which involves the first and higher harmonics in non-linear way. Only when the site energy splitting between copper and oxygen is by far the

largest energy in the problem, the tight-binding structure of the conduction band becomes an additive combination of low order Fourier harmonics. Here, we will point out that the topology of the measured Fermi surfaces, especially those of the weakly doped LSCO, suggests that the site energy splitting between copper and oxygen is not large. The analysis of the electric field gradients in the high- T_c superconductors [17] led to the same conclusion. Therefore we carefully examined the tight-binding band structure characterized with the Cu-O site energy splitting, the Cu-O hopping and the O-O hopping, for all the ratios of these three parameters. The agreement with the experiments turns out to be remarkably good, although our fits use small number of parameters, presumably because the non-linear dependence of the band structure on the first harmonics is properly taken into account.

The observation of the shadow bands in Bi2212 [4–6,8,9] opens the possibility that two of three tight-binding bands are present at the Fermi level. The range of parameters for which this can occur is determined here. In the three band model this is accompanied by the appearance of the extended van Hove singularities. It will turn out, however, that the topologies of these two tight-binding Fermi surfaces and the observed Fermi surfaces cannot be reconciled, suggesting that the shadow band in Bi2212 is the result of spin or of structure induced doubling of the BZ. This also means that in the three band model the extended van Hove singularities cannot occur close to the Fermi level, but the usual logarithmic singularities are expected to be strongly enhanced.

Surprisingly enough, the simple three band tight-binding model [18] has not been examined in sufficient

detail before. The previous attempts were focused on the correlation effects in the high- T_c oxides [19–23], examining the restricted range of the tight-binding parameters. It was concluded in particular that two lower bands can touch each other in the neighborhood of the Fermi level when the Cu-O site energy splitting and the oxygen-oxygen hopping are both positive [21]. Here we point out that such touching can occur for any relative sign of these parameters and even when the splitting vanishes. Small, doping dependant values of the renormalized Cu-O splitting are suggested by our comparison of the three band model with the ARPES data in the full range of the tight-binding parameters. This emphasizes the need for the correlation theory which leads to small, doping dependant values of the Cu-O splitting. It is interesting to note in this respect that the standard (the O-O hopping neglected) slave-boson mean field theory does lead to the effective Cu-O splittings which are small and even change sign for reasonable values of the bare tight-binding parameters [24]. The extensions of those results to the finite O-O hopping is therefore being carried out and will be presented in separate paper.

II. GENERAL

Here we examine the usual, nonmagnetic, undistorted CuO_2 square unit cell with $d_{x^2-y^2}$ ionic wave function associated to the Cu site, whereas the oxygen sites on the x and y axes are associated to the p_x and p_y states respectively. The phases of the wave functions are chosen as in Fig.1. Δ is the splitting between oxygen and copper site energies, $\Delta = \varepsilon_p - \varepsilon_d$.

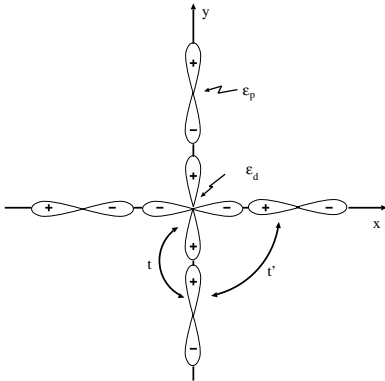


FIG. 1. Schematic representation of the CuO_4 plane defining the band parameters and the choice of the phases of the ionic wave functions

The hole picture is used here so that $\Delta > 0$ corresponds to the usually quoted values of $\varepsilon_p - \varepsilon_d$ [19] [21]. The hybridisations between Cu and O and between two neighbouring oxygens are introduced through the hopping integrals t and t' respectively. This simple picture

covers the noninteracting holes (electrons) in the CuO_2 plane, but also the case of the very large interaction U_d on the copper site, if the latter is treated by the mean-field slave boson approximation [19] or by the appropriate Hartree-Fock [21]. Both approximations lead to the renormalisation of the bare values of Δ and t , whereas t' is not affected by correlations. The Bloch states are built in the usual tight-binding way from $d_{x^2-y^2}$, p_x and p_y states in each unit cell and the band energies $\varepsilon_i(\mathbf{k})$ are found by diagonalisation of 3x3 hermitean matrix. This leads to the secular equation of the third order

$$\varepsilon^3 + 3p\varepsilon + 2q = 0 \quad (1)$$

where

$$p = -[\alpha + \beta(\eta^2 + \xi^2) + \gamma\eta^2\xi^2], \quad (2)$$

$$q = a + b(\eta^2 + \xi^2) + c\eta^2\xi^2, \quad (3)$$

with

$$\begin{aligned} a &= \frac{1}{27}\Delta^3, \quad b = \frac{2}{3}t^2\Delta, \quad c = -\frac{16}{3}t'[t'\Delta + 3t^2], \\ \alpha &= \frac{1}{9}\Delta^2, \quad \beta = \frac{4}{3}t^2, \quad \gamma = \frac{16}{3}t'^2, \end{aligned} \quad (4)$$

and

$$\eta = \sin \frac{k_x}{2}, \quad \xi = \sin \frac{k_y}{2}. \quad (5)$$

ε is the energy measured with respect to $\tilde{\varepsilon} = (\varepsilon_d + 2\varepsilon_p)/3$. The hermiticity of 3x3 tight-binding matrix ensures that three roots ε_i of Eq.(1) are real. It should be noted that Eq.(1) is invariant on the simultaneous replacement $\Delta \rightarrow -\Delta, t' \rightarrow -t'$ and $\varepsilon \rightarrow -\varepsilon$, irrespectively of the sign of t . This means that the band structure $\varepsilon_i(\mathbf{k})$ for $\Delta < 0, t' < 0$ or for $\Delta > 0, t' < 0$ can be obtained from the $\varepsilon_i(\mathbf{k})$ for $\Delta > 0, t' > 0$ or for $\Delta < 0, t' > 0$ respectively by the reflection on the \mathbf{k} plane. We shall therefore, without the loss of generality, carry out the theoretical discussion for $t, t' > 0$ and for both signs of Δ , although $t' < 0$ will also suit the experimental situation, as discussed in Section V. It can be finally noted that the band structure in the electron language, appropriate for the ARPES analysis is obtained from the band structure in the hole language used here by the reflection on the \mathbf{k} plane.

III. SMALL T'

It is instructive to start the discussion of the features of the energy bands by introducing t' as a small quantity. The well known results for $t' = 0$ are shown in Fig.2. For $\Delta > 0$ lower band ε_L is splitted from the intermediate and the upper band $\varepsilon_I, \varepsilon_U$ by Δ and the latter two bands,

ε_I being dispersionless, are degenerate at the Γ point. For $\Delta < 0$, the dispersionless band joins the lower band coinciding with it at the Γ point. The lowest band ε_L is half filled in the stoichiometric crystal, and the Fermi energy ε_F^0 coincides with the van Hove singularities at ε_x^L , for any value of t and Δ .

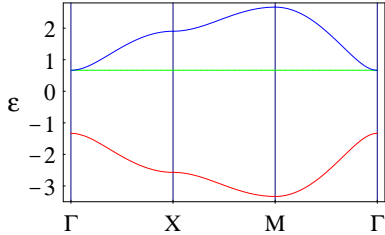


FIG. 2. Usual band structure when $t' = 0$, $\Delta > 0$, energy in units t

The small parameter t' can be introduced either by the usual perturbation theory applied to 3x3 tight-binding matrix or by iteration of the solutions of Eq.(1). Retaining only the leading term, linear in t' , (i.e. the first order perturbation theory) gives the structure of ε_L

$$\varepsilon_L(\mathbf{k}) = \varepsilon_L^0(\mathbf{k}) + \frac{32t't^2\eta^2\xi^2}{A(2A + \varepsilon_p + \varepsilon_d)}, \quad (6)$$

where

$$2A = \sqrt{\Delta^2 + 16t^2(\eta^2 + \xi^2)}. \quad (7)$$

The main qualitative effect of t' is the change in the number of the states below the van Hove singularity at ε_x^L , the value of which remains itself unaffected by t' . For $\Delta < 0$ or $\Delta > 0$ the number of the states below ε_x^L is increased or decreased respectively. In both cases the Fermi level ε_F^0 of the half-filled band is removed from the van Hove singularity at ε_x^L . The quantitative discussion is based on Fig.3.

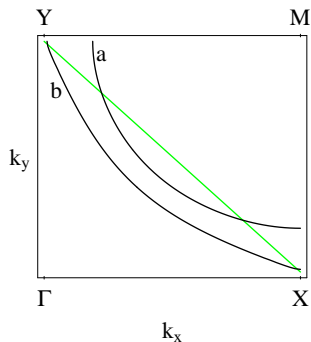


FIG. 3. Equienergetic contours of ε_L obtained for $\Delta < 0$ and small $t' \geq 0$; green - equienergetic line at $t' = 0$ that passes through van Hove points at ε_x^L , (a) - energy ε^0 that separates the states below and above it in two halves, (b) - equienergetic curve that passes through van Hove points

For $\Delta < 0$ the ε_x^L equienergetic straight line is bent towards the Γ point and all the states between this line and the finite t' curve are transferred from below ε_x^L to the energies above it. The number of the transferred states can be determined for small t' by expanding in terms of the small departure of the ε_x^L equienergetic curve for $t' \neq 0$ from the straight line and by calculating the surface between the straight line and this curve. Thus obtained number of the transferred states δ_c is

$$\delta_c = -\frac{4t'}{\pi^2 t} \text{sign}\Delta, \quad t' < |\Delta| < t, \quad (8a)$$

and

$$\delta_c = \frac{-8t'}{\pi^2 \Delta}, \quad t'|\Delta| < t^2 < \Delta^2. \quad (8b)$$

The energy ε^0 which divides the number of the states in the band in two halves can be calculated in the same spirit by finding the equienergetic curve which encompasses the same number of states below and above the straight line, as shown in Fig.3. For the two regimes considered above

$$(\varepsilon^0 - \varepsilon_x^L) \ln \frac{|\varepsilon^0 - \varepsilon_x^L|}{4t} = 2t' \text{sign}\Delta, \quad (9a)$$

and

$$\frac{\Delta(\varepsilon^0 - \varepsilon_x^L)}{t^2} \ln \frac{\Delta(\varepsilon^0 - \varepsilon_x^L)}{t^2} = \frac{16t'}{\Delta}. \quad (9b)$$

Note that ε^0 coincides with the Fermi level when the band ε_L is half filled, and then δ_c is the critical hole doping which brings the Fermi level to ε_x^L .

The number of the states δ between the two close energies ε and ε^0 can be determined by similar reasoning as

$$\varepsilon - \varepsilon^0 = \frac{\pi^2 t \delta}{2 \ln \frac{|\varepsilon^0 - \varepsilon_x^L|}{4t}} \text{sign}\Delta, \quad (10a)$$

and

$$\varepsilon - \varepsilon^0 = \frac{\pi^2 t^2 \delta}{8 \Delta \ln \frac{\Delta(\varepsilon^0 - \varepsilon_x^L)}{t^2}}. \quad (10b)$$

Obviously, Eq.(10) also defines the position of the Fermi level at $\varepsilon = \varepsilon_F$, if δ is taken to be the doping of the CuO_2 plane.

In two considered limits Eqs.(10) can be used to determine the density of states $d\delta/dE$ for ε between ε_x^L and ε^0

$$n_L(\varepsilon) = \frac{2}{\pi^2 t} \left(1 + \frac{2t'}{t}\right) \ln \frac{|\varepsilon - \varepsilon_x^L|}{4t}, \quad (11a)$$

and

$$n_L(\varepsilon) = \frac{|\Delta|}{2\pi^2 t^2} \left(1 + \frac{4t'}{|\Delta|}\right) \ln \frac{\Delta(\varepsilon - \varepsilon_x^L)}{t^2}, \quad (11b)$$

or vice versa, Eqs.(11) and (9) can be used to derive Eq.(10). The density of states between ε^0 and ε_x^L is increased by t' .

It should be noted that the results (9) to (11) concern only the energetic neighbourhood of the van Hove energy ε_x^L . The behavior of the band structure far from ε_x^L is irrelevant in this respect, in spite of the fact that t' leads to the level crossing for all the energies down to ε_M^L .

Let us close this discussion by noting that the density of states can be obtained from Eq.(6) in the closed form for all energies when $\Delta > t', t$. In this case, the spectrum of the lowest band can be obtained explicitly,

$$\varepsilon_L(\mathbf{k}) = -\frac{2}{3}\Delta + \frac{4t^2}{\Delta}(\eta^2 + \xi^2 - \frac{8t'}{\Delta}\eta^2\xi^2) \quad (12a)$$

in agreement with the usual additive form of the "tight-binding" fits. This leads to the density of states [25]

$$n_L(\varepsilon) = \frac{2|\Delta|}{\pi^2 t} \frac{1}{\sqrt{t^2 - 32t'\varepsilon}} \mathbf{K} \left[\frac{8\varepsilon(t^2|\Delta| - 4t't^2 - 2\varepsilon\Delta^2)}{t^3\sqrt{t^2 - 32t'\varepsilon}} \right] \quad (12b)$$

where the first term in Eq. (12a) is omitted and $K(x)$ is the complete elliptic integral of the first kind. For $t'|\Delta| < t^2 < \Delta^2$, Eq.(12b) reproduces the result (11b).

IV. BAND DEGENERACY

The main aim of the discussion which follows is to consider the degeneracies or the near degeneracies of the three bands ε_i , at a given \mathbf{k} , which are caused by including the oxygen-oxygen hopping t' into the dispersions in non-perturbative way. It is clear from Fig.3 that such effects can occur only when the dispersions related to t and t' are at least of the same order of magnitude, i.e. for the sufficiently large t' .

The large t' is also related to the qualitative modification of the dispersion within each band itself, e.g. the bending of the ε_x^L equienergetic line, instead of being small, as in Fig.3, becomes large, obviously changing the symmetry properties of the equienergetic surfaces all over the BZ. This is related to the fact that the O-O overlap induces the hopping along the diagonal of the Cu-O unit cell, unlike the Cu-O overlap, associated with the propagation along the cell's main axes, i.e. the additional propagation axes are rotated by $\pi/4$ with respect to the original ones.

As well known, the quantity proper to the study of the degeneracy of the spectrum ε_i at a given \mathbf{k} is

$$D = q^2 + p^3, \quad (13)$$

known as the discriminant of the third order Eq.(1). The hermiticity of the problem, i.e. of 3x3 tight-binding matrix, which makes the roots ε_i real, ensures that

$$D \leq 0 \quad (14)$$

For $D < 0$, all the roots ε_i are real and different, whereas $D = 0$, with $p^3 = -q^2 \neq 0$ implies that two roots are degenerate. For $p = q = 0$, all three roots coincide. Together with the inequality (14), this means that the zero of D at a given point \mathbf{k} of the BZ is also the maximum of D . Therefore, instead of the direct calculation of the zeroes of D , which is the third order polynomial in η^2 and ξ^2 , it is possible to find the optima of D with respect to η and ξ , and to determine which of those, if any, are the zeros of D . In carrying out this procedure, it is convenient to use the polar coordinates instead of η and ξ of Eq.(5)

$$\eta = \rho \sin \varphi, \quad \xi = \rho \cos \varphi. \quad (15)$$

The zero of the derivative of D with respect to φ is easily found to be

$$\begin{aligned} \frac{\partial D}{\partial \varphi} &= \rho^4 \sin 4\varphi \left[c(a + b\rho^2 + \frac{c\rho^4 \sin^2 2\varphi}{4}) \right. \\ &\quad \left. - \frac{3\gamma}{2} (\alpha + \beta\rho^2 + \frac{\gamma\rho^4 \sin^2 2\varphi}{4})^2 \right] = 0. \end{aligned} \quad (16)$$

The advantage of this representation is that, besides separating out immediately the trivial solution at $\rho = 0$, which corresponds to the degeneracy at the Γ point, it also exhibits other possible band degeneracies at $\varphi_{1,2} = 0, \pi/4$, i.e. on the $\Gamma\mathbf{X}$ and $\Gamma\mathbf{M}$ axes of the BZ.

The nature of the third maximum, associated with the zero of the square braces in Eq.(16) is best understood for $t = 0$, when this zero occurs for

$$\rho^2 \sin 2\varphi = \frac{|\Delta|}{2t'}. \quad (17)$$

This is easily recognized as the condition that the pure oxygen band crosses the dispersionless copper level, as shown in Fig.4. Consequently, $D_0 = D(t = 0) = 0$ on the line (17).

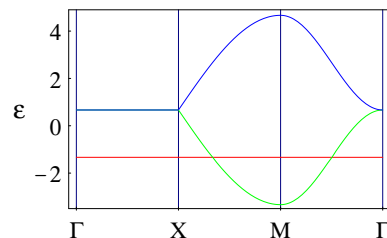


FIG. 4. Energy structure bands when $t = 0$, separated in two oxygen bands and the dispersionless copper level, energy in units t'

A. Lower critical value of t'

In the next step the change ΔD is calculated to the leading order in t . On the line (17)

$$\Delta D = -\frac{32}{27}\Delta^4 t^2 \left(\rho^2 - \frac{\Delta}{2t'}\right). \quad (18)$$

It follows that $\Delta D < 0$ in all the points on the crossing line (17) except for $\Delta > 0$ in the single point on the $\Gamma\mathbf{M}$ diagonal

$$\varphi_3 = \frac{\pi}{4}, \quad \rho_3^2 = \frac{\Delta}{2t'}, \quad (19)$$

where $\Delta D = 0$, i.e. $D = D_0 + \Delta D = 0$. The band degeneracy associated with the third maximum of D occurs on the $\Gamma\mathbf{M}$ diagonal and it is possible only for the same sign of Δ and t' . The variation of ΔD in the vicinity of the line (17) is weak with respect to the variation of $D_0 < 0$, i.e. $D = D_0 + \Delta D < 0$ in the vicinity of the line (17). Therefore, small t removes the degeneracy of two bands, except at the point (19), rather than displacing slightly the crossing line (17) to the new position. In other words, small t introduces the anticrossing of the oxygen band and the former copper level, excepting the single point (19) for $\Delta > 0$, as exemplified in Fig.5a and 5b.

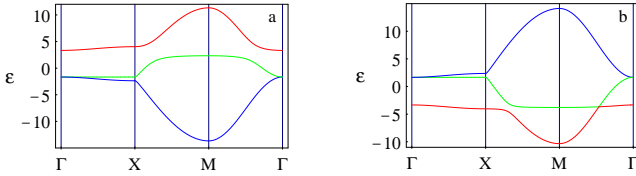


FIG. 5. Band anticrossing when $t'/t = 3$ and $\Delta/t = -5$ (a) and touching for $t'/t = 3$ and $\Delta/t = 5$ (b), energy in units t

Turning back to the first, $\varphi_1 = 0$ maximum of D , on the $\Gamma\mathbf{X}$ line, we note that for $t = 0$ it corresponds to the degeneracy of two oxygen bands, symmetric by reflection on the \mathbf{k} plane, while the dispersionless copper level is decoupled from the oxygen bands. When the copper is removed, the natural BZ corresponds to one oxygen per unit cell, i.e. it is rotated for $\varphi/4$ with respect to the original one and increased by $\sqrt{2}$. In this zone two bands unfold into one continuous oxygen band and the dispersionless $\Gamma\mathbf{X}$ line becomes analogous to the dispersionless straight line in Fig.3 for $t = 0$. The corresponding singularity in the density of states is therefore logarithmic [12,26]. For $t \neq 0$, the degeneracy on the $\Gamma\mathbf{X}$ line is removed, except in the Γ point, as shown e.g. in Fig.5b, with the consequences further discussed in Sec.V

The previous discussion shows that for finite t, t' the degeneracies of the bands at a given \mathbf{k} point can occur only on the $\Gamma\mathbf{M}$ line. Setting $\eta = \xi$ in the equation $D(\eta, \xi) = 0$ simplifies considerably further discussion. To this effect, it is convenient to distinguish between $\Delta > 0$ and $\Delta < 0$, as already suggested by Eq.(18) and start with the limit of small $|\Delta|$. The solution of the equation $D = 0$ is particularly simple around $\Delta = 0$ at the \mathbf{M} point of the BZ. By increasing t' from zero, the dispersionless oxygen level ε_I of Fig.2 bends towards the lower band ε_L and these two bands touch at the \mathbf{M} point. It can be shown analytically that, for $|\Delta|$ small, the degeneracy at the \mathbf{M} point occurs for

$$\frac{t'_{cr}}{t} = 0.5 + 0.167 \frac{\Delta}{t}, \quad (20)$$

i.e. for $\Delta > 0$ the oxygen level must bend more to cross the gap Δ than for $\Delta < 0$, when there is no gap to cross. Eq.(20) shows that the band touching occurs not only for $\Delta > 0$, as already known [21], but also for $\Delta < 0$. This is allowed by the solution $\varphi_2 = \pi/4$ of the Eq.(16), although the solutions $\varphi_3 = \pi/4, \rho_3$, given by Eq.(19), is not a zero of D when $\Delta < 0$. The full curve t'_{cr}/t versus Δ/t is obtained numerically in Fig.6. The limit of the large Δ/t in Fig.7 is transparent: it corresponds to the situation when the pure oxygen band touches the flat copper level at the \mathbf{M} point of the BZ. According to the Eq.(17), this occurs for $4t'_{cr} = \Delta$. In Fig.7a and 8a, the full three band structures, obtained by solving Eq.(1) numerically, are displayed for $\Delta/2t = \pm 0.5$ when $t'/t = t'_{cr}/2t = 0.64$ and 0.39 respectively.

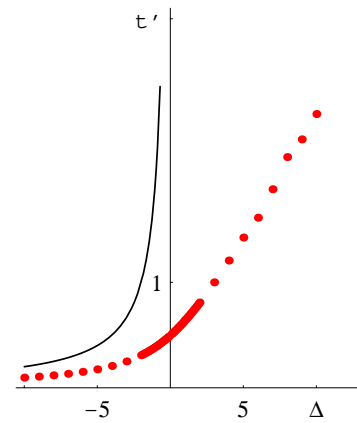


FIG. 6. For t' increasing from the lower critical value t'_{cr} to the upper critical value t'_{cr} the band touching that starts at the \mathbf{M} point moves along the $\Gamma\mathbf{M}$ line towards the Γ point. Limiting behaviors for small and large Δ/t described in the text are completed numerically (red dots). Δ and t' in units t .

$\Delta/2t = -1$ of Fig.8d.

B. Upper critical value of t'

It is further interesting to investigate what happens for $t' > t'_{cr}$ for the fixed value of $\Delta/t > 0$ in Fig.6. Some representative band structures are shown in Fig.7 for $\Delta/t = 1$. It appears that the bands ε_I and ε_L touch at a point which moves from the \mathbf{M} point towards the $\mathbf{\Gamma}$ point as t' increases from t'_{cr} . For $t'/t \gg 1$, the regime of the Eq.(17),(18) and (19) is reached, i.e. the touching of the bands occurs at $\rho^2 = \Delta/2t' < 1$.

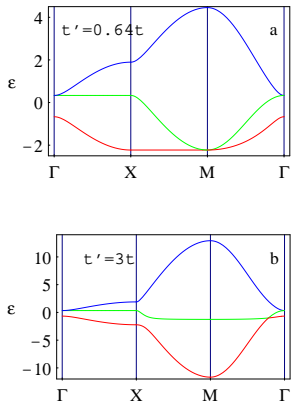


FIG. 7. Illustration of the touching of the two lower bands when t' and Δ are of the same sign for $\Delta/t = 1$. The touching point moves from \mathbf{M} point (a) towards $\mathbf{\Gamma}$ point (b), when the value of t' is increased from its critical value t'_{cr} . Energy in units t .

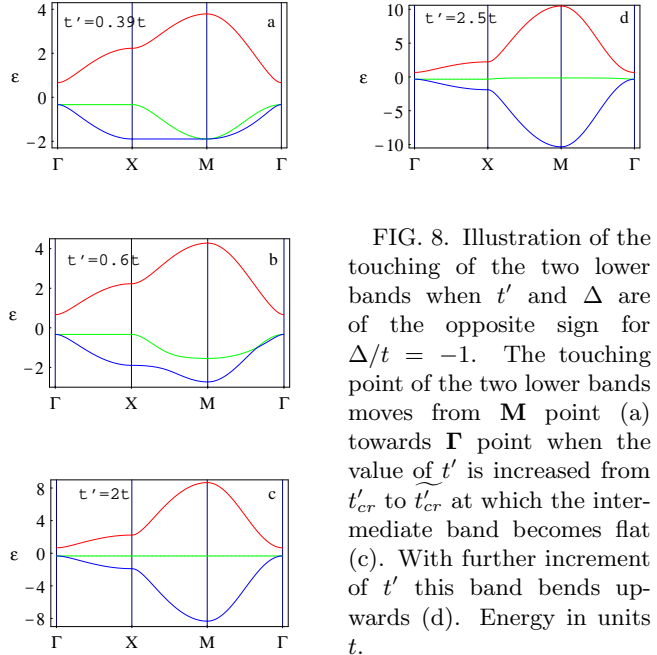


FIG. 8. Illustration of the touching of the two lower bands when t' and Δ are of the opposite sign for $\Delta/t = -1$. The touching point of the two lower bands moves from \mathbf{M} point (a) towards $\mathbf{\Gamma}$ point when the value of t' is increased from t'_{cr} to \tilde{t}'_{cr} at which the intermediate band becomes flat (c). With further increment of t' this band bends upwards (d). Energy in units t .

The situation is more complicated for $\Delta < 0$. It is illustrated in Fig.8 for $\Delta/t = -1$. As t'/t increases beyond \tilde{t}'_{cr}/t , the point of the coincidence moves towards the $\mathbf{\Gamma}$ point, reaching and leaving it for

$$\frac{\tilde{t}'_{cr}}{t} = -\frac{2t}{\Delta}. \quad (21)$$

For this value of parameters ε_I is again dispersionless as it was before for $t = 0$ in Fig.4. The corresponding dispersions of the bands ε_L and ε_U are given by

$$\varepsilon_{L,U} = -\frac{\Delta}{2} \left[1 \pm \sqrt{1 + \frac{16t^2}{\Delta^2} (\eta^2 + \xi^2 + 16\eta^2\xi^2)} \right]. \quad (22)$$

For $t' > \tilde{t}'_{cr}$, ε_I starts to bend towards ε_U and, according to the Eq.(19), reaches the anticrossing with this band at ρ^2 given approximately by Eq.(17). This anticrossing is more pronounced for $\Delta/2t = -5$ of Fig.5b than for

The discussion is completed by showing in Fig.9a, the band touching of Fig.8b with better resolution, the equienergetic surfaces of the bands ε_L and ε_I when they touch in the Fig.9b and the full dispersion of the bands ε_L and ε_I in Figs.9c and d. The topology of the bands on Fig.9b for $\Delta < 0$ shows striking similarity to the one found before for the bands that touch at $\Delta > 0$, i.e. the observation of such topology cannot be used to select the

sign of Δ .

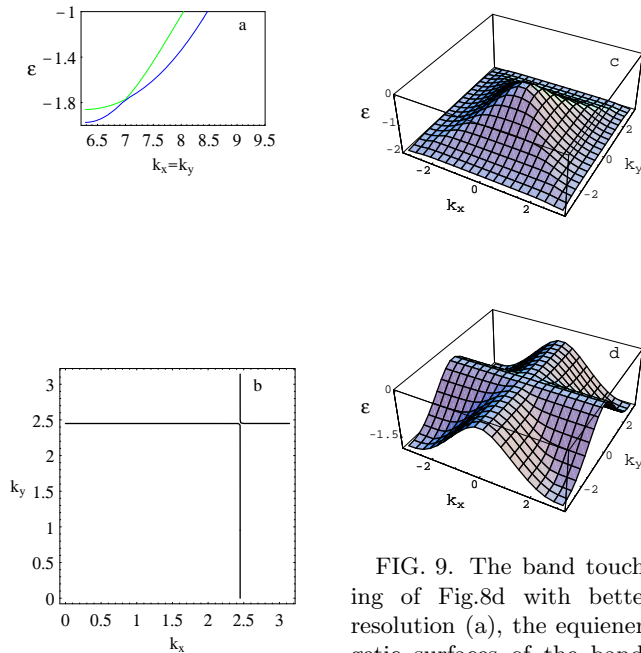


FIG. 9. The band touching of Fig.8d with better resolution (a), the equienergetic surfaces of the bands ε_L and ε_I when they touch (b) and the full dispersion of the bands ε_L and ε_I (c and d). Energy in units t .

C. $\Delta = 0$ bands

The features described above for $\Delta < 0$ and $\Delta > 0$ can be studied explicitly on the borderline $\Delta = 0$ between those two (cf. Fig.6) because then the electron spectrum can be obtained in the closed form

$$\varepsilon_L = -4t' \sqrt{\eta^2 \xi^2 + \frac{t^2}{4t'^2} (\eta^2 + \xi^2)} + \frac{t^2}{t'} \frac{\eta^2 \xi^2}{\eta^2 \xi^2 + \frac{t^2}{4t'^2} (\eta^2 + \xi^2)}, \quad (23a)$$

$$\varepsilon_I = \frac{-2t^2}{t'} \frac{\eta^2 \xi^2}{\eta^2 \xi^2 + \frac{t^2}{4t'^2} (\eta^2 + \xi^2)}, \quad (23b)$$

$$\varepsilon_U = 4t' \sqrt{\eta^2 \xi^2 + \frac{t^2}{4t'^2} (\eta^2 + \xi^2)} + \frac{t^2}{t'} \frac{\eta^2 \xi^2}{\eta^2 \xi^2 + \frac{t^2}{4t'^2} (\eta^2 + \xi^2)}. \quad (23c)$$

for $t' \gg t$ and similarly for $t' \ll t$.

Eqs.(6),(22) and (23) illustrate the fact that in the tight-binding approximation the spectrum is built from low order harmonics η^2 , ξ^2 of the Eq.(5) in nonlinear way. Eq.(23) and (24) are useful also because it will turn out in Sec.VI that the experimental spectra are close to the $\Delta = 0$ limit.

V. EXTENDED VAN HOVE SINGULARITIES

Inspection of Figs.7 and 8 shows that the degeneracy of the bands ε_L and ε_I at the point \mathbf{M} , for $t' = t'_{cr}$ is accompanied in the band ε_L with the absence of the dispersion on the line between Γ and \mathbf{M} points. It appears that the dispersion depends only on the component of the wavevector perpendicular to the $\Gamma\mathbf{M}$ line, in a quadratic way, i.e. the dispersion is one-dimensional on whole $\Gamma\mathbf{M}$ line. As a result, an "extended" van Hove singularity is found in the density of states [3,14,15] of the lowest band

$$n_L(\varepsilon) \approx \frac{B}{\sqrt{\varepsilon - \varepsilon_L^M}}. \quad (24)$$

When the degeneracy between the Γ and \mathbf{M} points is lifted by changing slightly t' from t'_{cr} , the usual step singularity at ε_M^L and the logarithmic singularity at ε_x^L are recovered in $n_L(\varepsilon)$, lying close to each other in energy, i.e. enhancing each other. The described coalescence of these two singularities can be explicitly found in Eq.(12), but it occurs there for $-8t' = \Delta$, when, unfortunately, the expansion in terms of $|\Delta| \gg t, t'$ is only qualitatively correct.

Similar extended van Hove singularities are associated with the absence of the dispersion on the $\Gamma\mathbf{X}$ line in the band ε_I for any finite values of t and t' . For $t = 0$ however, as already explained below Eq.(18), the copper level is decoupled from the oxygen band structure and two oxygen bands ε_I and ε_U coalesce into one band with the artificial degeneracy on the $\Gamma\mathbf{X}$ line. When the artificial degeneracy is removed, by increasing the BZ so that it corresponds to one oxygen per unit cell, the spectrum of this band is continuously increasing through the $\Gamma\mathbf{X}$ line, what is thus associated with the logarithmic, and not with the extended van Hove singularity in the density of states.

It is apparent here that in the three band model with $1 + \delta$ holes, the Fermi level falls far from the extended van Hove singularity in the ε_I band. On the other hand, when the extended van Hove singularity (24) occurs for $t' = t'_{cr}$ in the ε_L band, the Fermi level crosses necessarily two bands, ε_L and ε_I . This fact makes the discussion of the main band and the shadow bands, observed in some of the high- T_c superconductors [4-6,8,9], quite relevant. The rest of this paper is devoted to the analysis of the empirical band structure. As already mentioned, it will turn out that the observed dispersions of the main band and the shadow band cannot be reconciliated with $\varepsilon_L(\mathbf{k})$ and $\varepsilon_I(\mathbf{k})$, i.e. the extended van Hove singularities of the three band model do not occur close to the Fermi level.

VI. EXPERIMENTS

The previous discussion provided the complete description of the three band structure. Although it was carried out for $t' > 0$ and arbitrary sign of Δ , the symmetry properties (cf Sec.II) extend it to the entire range of the parameters. In this section, we shall compare these results with the experimental data obtained by the ARPES measurements.

The first step is to determine the position of the Fermi level ε_F for the doping δ in the calculated band structure, then to find the corresponding Fermi surface and finally to compare it with the empirical data. Since the discussion was carried out in the hole picture, $1 + \delta$ holes are placed in the lowest band beginning from its bottom at the (π, π) point, (i.e. the **M** point of the square unit cell), to the Fermi level ε_F , where ε_I is also possibly present for $t' > 0$. As already mentioned in Sec.II, the band structure for $t' < 0$ can be obtained from the one calculated for $t' > 0$ by the reflection on the \mathbf{k} plane. The result is that ε_F falls then in the ε_U band alone, i.e. the band touching cannot occur close to the ε_F . In any case, all three bands can be brought to the Fermi level of $1 + \delta$ holes by varying appropriately the tight-binding parameters.

Using in particular the regime separation summarized in Fig.6, all the regimes of the parameters are examined in this way, comparing the topology of the obtained Fermi surfaces with the corresponding experimental data. The bending of the Fermi surfaces towards the Γ point requires that Δ and t' have the opposite signs for all the considered materials. This is already apparent in the small t' limit of Sec.III and generalizes to arbitrary t' . The values of the parameters vary among different materials as will be discussed below. It is also appropriate to point out that all the experimentally obtained Fermi surfaces are fitted here with only two different parameters, e.g. with $t/2t'$ and $\Delta/2t'$. Two more parameters, e.g. t and $\tilde{\varepsilon} = (\varepsilon_d + 2\varepsilon_p)/3$ are needed to fit the conducting band(s) away from ε_F .

A. $\text{La}_{2-x}\text{Sr}_x\text{CuO}_4$

The recent ARPES measurements in LSCO [10,11] give the evolution of the Fermi surface in the large range of dopings δ . The two parameters fit of those data are shown in Fig.10a–e. Two sets of fitting parameters, given in Fig.11, one characterized by $t' > 0$, $\Delta < 0$ and the other by $t' < 0$, $\Delta > 0$, fit the data equally well. It follows that the rigid band model is completely inadequate to describe the evolution of the Fermi surface with δ , because in both sets $\Delta/2t'$ and $t/2t'$ undergo large

variations with δ .

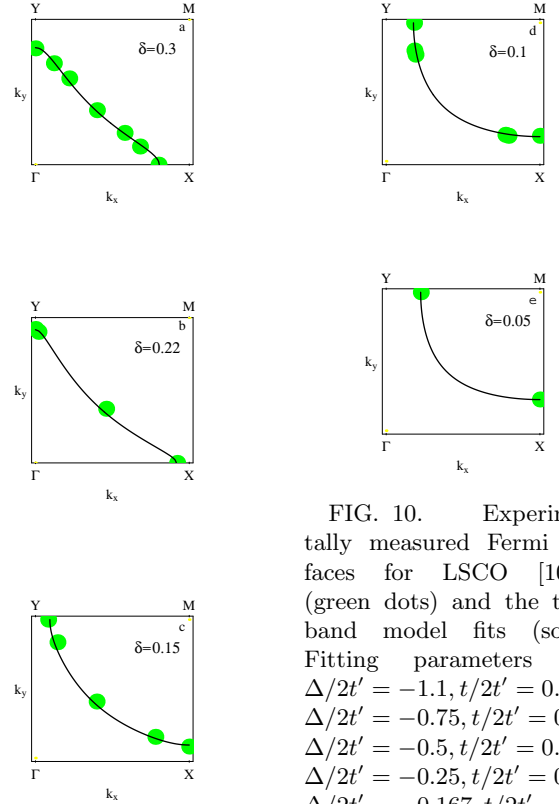


FIG. 10. Experimentally measured Fermi surfaces for LSCO [10,11] (green dots) and the three band model fits (solid). Fitting parameters are: $\Delta/2t' = -1.1$, $t/2t' = 0.56$ (a), $\Delta/2t' = -0.75$, $t/2t' = 0.5$ (b), $\Delta/2t' = -0.5$, $t/2t' = 0.42$ (c), $\Delta/2t' = -0.25$, $t/2t' = 0.25$ (d), $\Delta/2t' = -0.167$, $t/2t' = 0.167$ (e)

It is further important to note in Fig.11 that for both sets of parameters $\Delta/2t'$ and $t/2t'$ are small for small δ . This is best understood by noting that for $\Delta = 0$, $t = 0$ the Fermi surface of the half-filled ($\delta = 0$) band coincides with k_x , k_y axes of the BZ, which in the qualitative terms corresponds to the Figs.10a–e. As already explained in Sections III and V, the energetic degeneracy of the $\Gamma\mathbf{X}$ line in the pure ($t = 0$) oxygen model is related to the logarithmic rather than to the extended van Hove singu-

larity in the density of states.

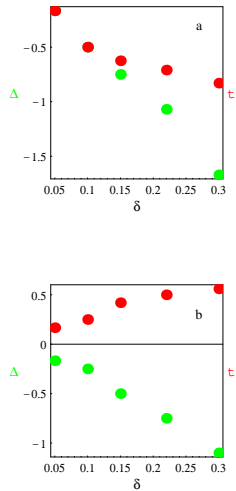


FIG. 11. Two sets of the fitting parameters with $\Delta > 0$, $t' < 0$ (a) and $\Delta < 0$, $t' > 0$ (b) in units $2t'$, that fit the experimentally obtained Fermi surfaces [10,11] of LSCO, shown on Figs. 10a-e, equally well. For $\delta = 0.05$ and $\delta = 0.1$ on the Fig.11a, $\Delta/2t'$ and $t/2t'$ have the same values.

The full band structure with Δ and t small, but finite is shown in the Fig.12 for $\Delta < 0$, $t' > 0$. In particular Figs.12e and d illustrate that weak dispersion is introduced by t in the conducting band ε_L along the $\Gamma\mathbf{X}$ line, i.e. the van Hove singularity at \mathbf{X} , although enhanced, is logarithmic. Fig.12 also shows that for the values of parameters found in the case $\Delta < 0$, $t' < 0$ the band ε_I is rather far from the Fermi level. For $\Delta > 0$, $t' > 0$, this holds independently on the values of the parameters.

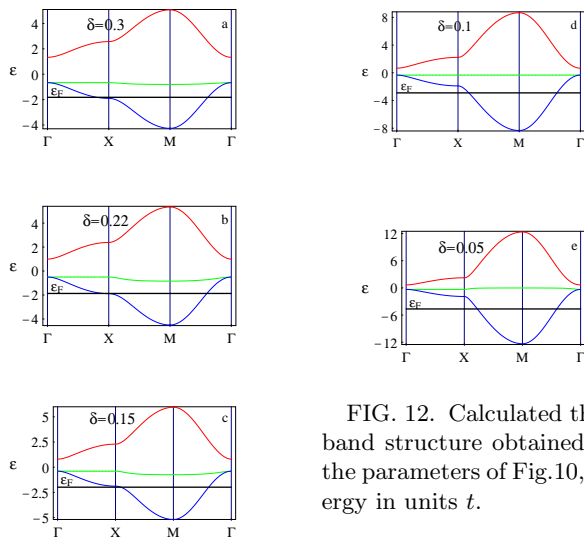


FIG. 12. Calculated three band structure obtained for the parameters of Fig.10, energy in units t .

The usual $t' = 0$ mean field slave boson theory with large U , other interactions absent, allows small and even negative values of Δ [24], but large variations of Δ and t with the doping δ are not obtained this way. The slave boson calculations with finite t' are under way for this reason and also because the previous results with finite

t' do not cover the range of parameters which appeared to be relevant here.

B. $\text{Bi}_2\text{Sr}_2\text{CaCu}_2\text{O}_8$

As interesting feature of the ARPES results in Bi2212 taken in the normal state is the appearance of two Fermi surfaces in the BZ [4–6,8,9]. There are points in the 2d \mathbf{k} space in which two Fermi lines cross or touch. In the three band model such points can occur only on the $\Gamma\mathbf{M}$ line, as shown in Figs.7,8 and 9, whereas the experimental crossing or touching points fall quite far from this line. It is therefore more appropriate to interpret two observed Fermi lines as belonging to the main band of the same topology as the one found in LSCO, and to the shadow band obtained by the (π, π) shift of the main band. It is likely that this shift is produced by AF or by structural (π, π) superlattice. The values of parameters which fit the main band are $\Delta/2t' = -0.0625$ and $t/2t' = -0.1$, i.e. Bi2212 has even smaller values of Δ and t than LSCO with $\delta \approx 0.05$. However, the number of holes $1 + \delta$ below Fermi level corresponds to $\delta \approx 0.25$. Similar conclusion holds also for $\Delta < 0$, $t' > 0$.

In addition to the Fermi surfaces the ARPES measurements in Bi2212 provide the information about the states filled with electrons, i.e. about the empty hole states [16]. When the fit is extended to the energies away from the ε_F , $\tilde{\varepsilon}$ and t are determined. The best fits to those measurements are shown in Fig.13b. The idea underlying these fits is that the Fermi liquid theory applies to the effects of magnetic, structural or superconducting fluctuations, beyond the mean field slave boson theory. The latter gives only the basic band structure, which was discussed here. The Fermi liquid renormalisation of this structure by fluctuations presumably vanish at ε_F , i.e. the band theory is accurate at ε_F [27], as it is implicit from the fits of the Fermi surfaces, given in Figs.10 and 13. The departures of the experimental data from such fits are thus to be associated with the fluctuation effects

away from ε_F .

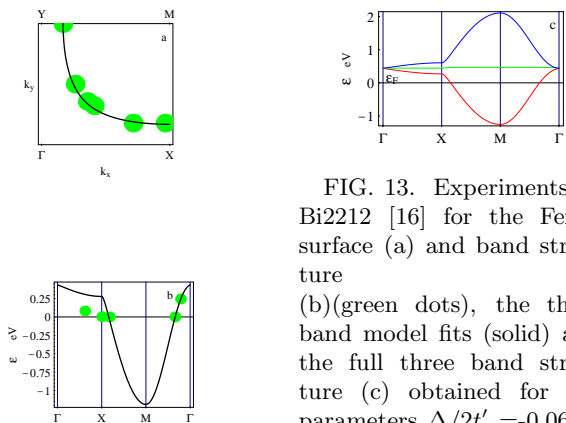


FIG. 13. Experiments in Bi2212 [16] for the Fermi surface (a) and band structure

(b)(green dots), the three band model fits (solid) and the full three band structure (c) obtained for the parameters $\Delta/2t' = -0.0625$, $t/2t' = -0.1$, $\tilde{\varepsilon} = 0.44\text{eV}$ and $t = 0.08\text{eV}$

The most prominent fluctuation effect defined this way is the flattening of the measured dispersion along the **XM** line, compared to the band model prediction (Fig.14b). This flattening is understood here as the precursor of the gap opening around the **X** point, which is observed e.g. on doping Bi2212 with Dy [28]. The precursor is not expected to be a simple pseudogap, which occurs only when the adiabatic approximation can be applied to the relevant fluctuations. Due to the small velocity of electrons, the adiabatic approximation fails in the van Hove singularity, and the band states are conserved at the Fermi level, although a part of them can be transferred to the pseudogap wings. This theoretical prediction, which justifies the description of the Fermi surface by the band theory, is borne out by the recent high resolution ARPES measurements along the **ΓX** line [29]. Those data show empirically that the states close to ε_F in the vicinity of the **X** point are shared between the peak at ε_F and the pseudogap wings. The calculations of the detailed **k** dependences and the comparison with the experiments is currently under way.

C. $\text{YBa}_2\text{Cu}_3\text{O}_{6.95}$

There are two planes per unit cell of Y123 which result in dimerisation of the CuO_2 bands along the axis perpendicular to the planes. In addition, the CuO chains of Y123 are conducting, which complicates further the analysis of the observed band structure. It is however reasonable to assume that the lowest of the CuO_2 bands undergoes only the dispersionless dimerisation shift towards lower energies.

The fit of the lowest band measured in Y123 [1,2] with the three band model, shown in Fig.14, proceeds similarly to the cases of LSCO and Bi2212. The Fermi surface

fit leads to $\Delta/2t' = -0.0625$, $t/2t' = -0.1$ i.e. to the values characteristic for Bi2212. It is interesting to note that the band flattening observed in Bi2212 along the **XM** line does not occur in Y123. If not a problem of the experimental resolution, this suggests that the nature of fluctuations which affect the vicinity of the **X** point in the electron spectrum differs considerably between Bi2212 and Y123 and opens an interesting question which requires further investigation.

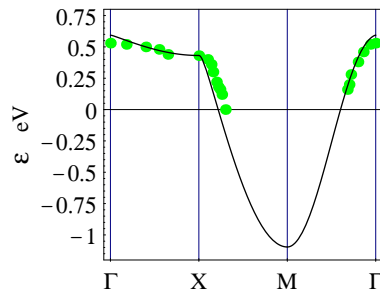


FIG. 14. Experimentally measured structure of the lowest band of Y123 [1] (green dots) and the three band model fits (solid) with parameters $\Delta/2t' = -0.0625$, $t/2t' = -0.1$, $\tilde{\varepsilon} = 0.58\text{eV}$ and $t = 0.08\text{eV}$

VII. CONCLUSION

In contrast to the most of the many body theories of the high- T_c superconductors, which are attempting to construct the electron band structure starting from a given set of bare band and interaction parameters, this paper assumes that the resulting average band structure can be described with a few effective near-neighbor tight-binding parameters. After the detailed analysis, which encompasses the rich structure of the three band model, it appears that the single band at the Fermi level describes the Fermi surfaces in LSCO, Bi2212 and Y123 remarkably well. Only two parameters are used in those fits, compared to the usual, at least four parameter fits of the Fermi surfaces. The improvement is obtained by the use of the effective tight-binding band structure which is non-linear in low order harmonics in contrast to the Fourier fits. This indicates that the average band structure arises from the (large) short range correlations. The departure of the predicted band behavior, measured in the vicinity the Fermi level, is used to determine the effects of the fluctuations on the small energy scales not included in the average band structure. This way the desired results of the many body theories are defined more clearly, they should end up with the effective tight-binding parameters in the energy range between 1eV and 0.1eV, and with the additional fluctuation effects on the

energy scales of the order of 0.1eV to 0.01eV. The corresponding space scales of the correlations involved into the average band structure and into departures from it are related in analogous way. Large energy scales alone describe the Fermi surface, what implies that the Fermi liquid theory is the good starting point in the calculation of the fluctuation effects.

VIII. ACKNOWLEDGMENT

We would like to thank Prof. Jacques Friedel, Dr. Davor Pavuna, Dr. Eduard Tutiš, Dr. Denis Sunko and Dr. Ivan Kupčić for the stimulating discussions. This work was supported by Croatian Ministry of Science under the project 119-204.

* e-mail: ivanam@phy.hr

- [1] M.C.Shabel, C.-H. Park, A. Matsuura, Z.-X. Shen, D.A. Bonn, Ruixing Liang and W.N. Hardy, Phys. Rev. B **57**, 6090 (1998)
- [2] M.C.Shabel, C.-H. Park, A. Matsuura, Z.-X. Shen, D.A. Bonn, Ruixing Liang and W.N. Hardy, Phys. Rev. B **57**, 6107 (1998)
- [3] K.Gofron, J.C. Campuzano, A.A. Abrikosov, M. Lindroos, A. Bansil, H. Ding, D. Koelling and B. Dabrowski, Phys. Rev. Lett. **73**, 3302 (1994)
- [4] P.Aebi, J. Osterwalder, P. Schwaller, L. Schlapbach, M. Shimoda, T. Mochiku and K. Kadowaki, Phys. Rev. Lett. **72**, 2757 (1994)
- [5] H.Ding, A.F. Bellman, J.C. Campuzano, M. Randeria, M.R. Norman, T. Yokoya, T. Takahashi, H. Katayama-Yoshida, T. Mochiku, K. Kadowaki, G. Jennings and G.P. Brivio, Phys. Rev. Lett. **76**, 1533 (1996)
- [6] J.Mesot, M.R. Norman, H. Ding and J.C. Campuzano, Phys. Rev. Lett. **82**, 2618 (1999)
- [7] Y.-D. Chuang, A.D. Gromko, D.S.Dessau, Y. Aiura, Y. Yamaguchi, K. Oka, A.J. Arko, J. Joyce, H. Eisaki, S.I. Uchida, K. Nakamura and Yoichi Ando, Phys. Rev. Lett. **83**, 3717 (1999)
- [8] H.M.Fretwell, A. Kaminski, J. Mesot, J.C. Campuzano, M.R. Norman, M. Randeria, T. Sato, R. Gatt, T. Takahashi and K. Kadowaki, Phys. Rev. Lett. **84**, 4449 (2000)
- [9] S.V.Borisenko, M.S. Golden, S. Legner, T. Pichler, C. Durr, M. Knupfer, J. Fink, G. Yang, S. Abell and H. Berger, Phys. Rev. Lett. **84**, 4453 (2000)
- [10] A.Ino, C. Kim, T. Mizokawa, Z.-X. Shen, A. Fujimori, M. Takaba, K. Tamasaku, H. Eisaki and S. Uchida, J. Phys. Soc. Jpn. **68**, 1496 (1999)
- [11] A.Ino, C. Kim, M. Nakamura, T. Yoshida, T. Mizokawa, Z.-X. Shen, A. Fujimori, T. Kakeshita, H. Eisaki and S. Uchida, cond-mat/0005370 (2000)
- [12] J.Labbé and J.Bok, Europhys. Lett. **3**, 1225 (1987)
- [13] S.Barišić, I. Batistić and J. Friedel, Europhys. Lett. **3**, 1231 (1987)
- [14] A.A.Abrikosov, J.C. Campuzano and K. Gofron, Physica C **241**, 73 (1993)
- [15] A.A.Abrikosov, Physica C **341**, 97 (2000)
- [16] M.R.Norman, M. Randeria, H. Ding and J.C. Campuzano, Phys.Rev.B**52**,615(1995)
- [17] I.Kupčić, S. Barišić and E. Tutiš, Phys. Rev. B **57**, 8590 (1998)
- [18] V.J. Emery, Phys. Rev. Lett. **58**, 2794 (1987)
- [19] Ju H. Kim, K.Levin and A. Auerbach, Phys. Rev. B **39**, 11633 (1989)
- [20] Qimiao Si, Yuyao Zha, K. Levin and J.P.Lu, Phys. Rev. B **47**, 9055 (1993)
- [21] D.I.Golosov, A.E.Ruckenstein and M.L.Horbach, J. Phys.: Condens. Matter **10**, L229 (1998)
- [22] J.K.Perry and J.Tahir-Kheli, Phys. Rev. B **58**, 12 323 (1998)
- [23] J.K.Perry and J.Tahir-Kheli, cond-mat/9908308 (1999)
- [24] E.Tutiš, Ph.D. thesis, University of Zagreb (1994)
- [25] D.Y.Xing, M.Liu and C.D.Gong, Phys. Rev. B **44**, 12525 (1991)
- [26] J.Bok, J. Supercond. **7**, 547 (1994)
- [27] D.K.Sunko and S.Barišić, Europhys. Lett. **22**, 299 (1993)
- [28] D.S.Marshall, D.S. Dessau, A.G.Loesser, C.-H. Park, A.Y. Matsuura, J.N. Eckstein, I. Bozovic, P. Fournier, A. Kapitulnik, W.E. Spicer and Z.-X. Shen, Phys. Rev. B **76**, 4841 (1996)
- [29] S.Rast, B.H. Frazer, M. Onellion, T. Schmauder, A. Abrecht, O. Touzelet, H. Berger, G. Margaritondo and D. Pavuna, Europhys. Lett **1**, 103 (2000)